Powder Technology 310 (2017) 1–7

Contents lists available at ScienceDirect

Powder Technology

journal homepage: www.elsevier.com/locate/powtec

Effects of mud slurry on flow resistance of cohesionless coarse particles

Hongjuan Yang [a,b,*], Fangqiang Wei [b], Kaiheng Hu [b], Juan Lyu [b]

[a] Key Laboratory of Mountain Hazards and Earth Surface Process, Chinese Academy of Sciences, Chengdu 610041, China
[b] Institute of Mountain Hazards and Environment, Chinese Academy of Sciences, Chengdu 610041, China

ARTICLE INFO

Article history:
Received 19 September 2016
Received in revised form 6 January 2017
Accepted 8 January 2017
Available online 10 January 2017

Keywords:
Mud slurry
Cohesionless particles
Excess pore fluid pressure
Flow resistance
Rheology

ABSTRACT

Laboratory experiments were performed to investigate the effect of mud slurry on the flow resistance of cohesionless particles in debris flow. For one thing, natural angles of repose were measured for the gravel materials resting in air, in water, and in mud slurry separately. For another, rheological tests were taken using a vane rheometer to measure the torque-time response of sand particles within mud slurries of varying solid concentrations both at low and high rotational speeds. The stable torque obtained at the low rotational rate, which represents flow resistance primarily caused by particle contact friction, was nondimensionalized to compare the internal friction coefficient in each case. Furthermore, flow resistance of sand particles within one of the mud slurries was measured over a wide range of rotational speeds to compare with that in the dry system. It was found that the mud slurry has no significant effects on the frictional coefficient of cohesionless coarse particles. However, the mud slurry tends to decrease flow resistance of the particles, with the effect being more significant at higher rotational speeds or for more concentrated slurries. This derives from excess pore fluid pressure, which is easier to maintain at higher shear rates or within more cohesive slurries.

1. Introduction

Debris flow is a natural phenomenon with the flow behavior between those of hyper-concentration flow and landslide. The solid fraction in debris flow has a wide size distribution varying from clay particles to boulders. It is not uncommon to regard debris flow as pseudo-homogeneous and describe its behavior with rheological models. This method encounters difficulties in explaining some complex phenomena with debris flow, such as particle size segregation [1]. As a result, two-phase fluid models have been increasingly employed in dynamic simulation of debris flow [2–4]. In such models, the fluid phase is comprised of water and fine particles homogeneously dispersed in water, while coarser particles constitute the solid phase [5]. Both Bingham model and Herschel-Bulkley model are widely utilized to characterize rheological properties of the fluid phase [6]. A number of studies have focused on this issue and reveal that the rheological parameters are influenced by such factors as particle size distribution, solid volume concentration, and mineral composition [7–8]. Particles that comprise the solid phase of debris flow are cohesionless. Their flow characteristics are similar to that of granular flow, in which field paramount progress has been achieved in recent years, including the rheological expression in flow resistance of monodisperse particles [9–10] and particle size segregation in polydisperse granular avalanches [11–12]. For debris flow, clay particles are included in the fluid phase. Flume experiments suggest that the existence of a certain fraction of clay minerals contributes to maintaining excess pore water pressure in debris flow and thus enhances its mobility [13–14]. Consequently, influences exerted by the fluid phase on flow resistance of the solid phase should be taken into account.

Some researchers have conducted studies regarding effects of interstitial fluid on granular flow. Experiments on granular matter in Newtonian fluids in a rotating drum reveal that velocities of the particles decrease with increasing fluid viscosity, while the angle of repose with a liquid interstitial fluid is larger than that for the dry system [15–16]. Using a pressure-imposed shear cell, Boyer et al. [17] study the rheology of cohesionless particles dispersed in a fluid with the same density as the particle and establish relationships of the frictional coefficient and the solid volume concentration with a dimensionless viscous number. Fluids employed in these studies were Newtonian. In contrast, the fluid phase in debris flow is mud slurry which exhibits yield stress and probably produce different impacts on flow behaviors of granular matter. In this respect, experiments conducted by Ancey [18] provide some valuable results. Making use of vane rheometry, Ancey [18] investigates the bulk behavior of concentrated suspensions of coarse and fine (colloidal) particles in water and finds that the bulk behavior varies both with the concentration of fine particles and the shear velocity.

The present research mainly refers to the method used by Ancey [18] and studies effects of mud slurry on the flow resistance of granular matter. Instead of paying attention to flow behaviors of the suspensions, we focus on comparing the flow resistance of cohesionless particles in mud

* Corresponding author at: Key Laboratory of Mountain Hazards and Earth Surface Process, Chinese Academy of Sciences, Chengdu 610041, China.
E-mail address: yanghj@imde.ac.cn (H. Yang).

http://dx.doi.org/10.1016/j.powtec.2017.01.036
0032-5910/

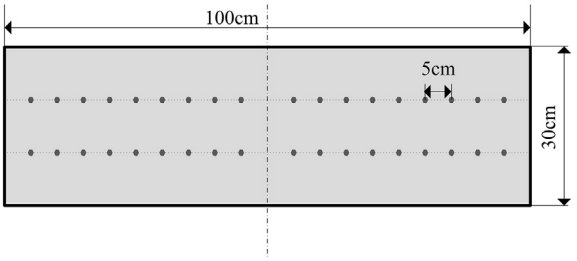

Fig. 1. Measurement positions with the thread method.

slurries of different concentrations. In this paper, Section 2 introduces experimental materials and procedure, while Section 3 analyzes the results following which is the conclusion part.

2. Experimental procedures

2.1. Experiment on the angle of repose

For cohesionless particles, the angle of internal friction approximately equals the natural angle of repose [19]. As a consequence, effects of mud slurry on the internal frictional angle of granular matter could be preliminarily examined by comparing the natural angles of repose measured in air, in water, and in the mud slurry, respectively.

2.1.1. Materials

To prepare the slurry, we used the fine fraction (<1 mm) in the debris flow sediment sampled from Jiangjia Gully, Yunnan Province, China. According to the measurement by a Mastersizer 2000 laser particle size analyzer, the median particle size of the material is 0.022 mm, with clay minerals (<0.005 mm) accounting for 24.8%. The particle density is 2752 kg/m^3. Dongchuan Debris Flow Observation and Research Station, Chinese Academy of Sciences has carried out observation at Jiangjia Gully for >50 years. Measurement data show that in viscous debris flows, the densities of which are >2000 kg/m^3 [20], the solid volume concentration in slurry suspensions comprised of fine particles (<1 mm) and water changes from 0.248 to 0.443, with an average of 0.349. Based on the average concentration, we prepared the mud slurry with a bulk density of 1611 kg/m^3. All the fine particles could maintain suspended for a long time in the slurry. Gravels of 10–20 mm in size were used as coarse particles in this experiment. The particle density is approximately 2750 kg/m^3. These gravels could settle immediately in the slurry.

2.1.2. Experimental setup and procedure

The experiment was performed in a horizontal glass tank, which is 100 cm long, 30 cm wide and 70 cm deep. Considering the nontransparent feature of the slurry, we used the following procedure to get the natural repose angle of gravels in the slurry: (1) prepare the slurry and pour it into the tank, then mix the slurry thoroughly by hand; (2) pour the gravels into the slurry gradually along the central line of the tank surface (Fig. 1), thus a sediment deposit is formed; (3) use a fine thread (0.25 mm in diameter) tied to a steel bead (20 mm in diameter) on one end to measure the distance between the deposit surface and the tank surface at specific positions, which are 1/3 or 2/3 of the width to the long side wall of the tank with an interval of 5 cm, as illustrated in Fig. 1; (4) plot the measurement data versus the distance between the measurement position and the short side wall of the tank, and then fit data points with a straight line, thus achieving the angle of repose. When measuring the angles of repose in air and in water, the same procedure was followed except step (1). For convenience, this method for determining the angle of repose is called thread method.

To check accuracy with the thread method, the triangle method was also employed when determining the angles of repose in air and in water. In this method, a triangle was depicted on the wall following the deposit surface [19], as shown in Fig. 2. Therefore, for coarse particles depositing in air or in water, we got four angle values with each method in one test. For these cases, the test was repeated once. For gravels depositing in the slurry, there were no repeated tests. Nevertheless, in this case additional measurements were performed at positions that were 1/6, 1/2, or 5/6 of the width to the long side wall of the tank, thus generating ten angle values in total.

2.2. Rheological experiment

2.2.1. Materials

Mud slurries in the rheological experiment were prepared with finer particles (<0.075 mm in diameter) than that used in the experiment on the natural angle of repose. These materials were also collected from Jiangjia Gully. The particle density is 2752 kg/m^3 and the median particle size is 9.5 μm. Six different slurries were made with the solid volume concentration C_{vf} ranging from 0.048 to 0.292, as listed in Table 1. Rheological tests were performed on these slurries with the roughened concentric cylinder system of an Anton Paar Physica MCR301 rheometer (radius of the rotor: 15.22 mm, length of the rotor: 45.60 mm, radius of the cup: 21.00 mm, roughness: 0.5 mm). The curve of shear stress versus shear strain was used to derive yield stress [21]. Repeated tests

Fig. 2. Sketch map of the triangle method.

Table 1
Characteristics of materials employed in the rheological experiment.

Sample number	C_{vf}	ρ_f (kg/m^3)	τ_{yf} (Pa)	C_{vc}	C_{vt}	N
1	0.000	0	0.00	0.506	0.506	–
2	0.000	997	0.00	0.506	0.506	–
3	0.048	1082	0.08	0.506	0.530	32.0
4	0.097	1166	0.09	0.506	0.554	28.5
5	0.145	1252	0.35	0.506	0.578	6.6
6	0.194	1337	0.70	0.506	0.602	3.1
7	0.243	1423	2.22	0.506	0.626	0.9
8	0.292	1509	5.33	0.474	0.627	0.3

C_{vf} is solid volume concentration in the mud slurry, ρ_f is bulk density of the mud slurry, τ_{yf} is yield stress of the mud slurry, C_{vc} is the volume concentration of coarse particles in the whole mixture, C_{vt} is the total solid concentration, and N is a dimensionless number as defined by Eq. (1).

showed an acceptable repeatability (<20%). Table 1 illustrates the average yield stress of each slurry.

Silica sands with the size of 0.5–1 mm were employed as coarse particles in the rheological experiment. The particle density is 2646 kg/m^3. A preliminary test showed that the volume concentration of the sand particles shaken by hand for 1 min after random loose packing was approximately 0.506. As a result, the volume concentration of coarse particles C_{vc} was set at 0.506 in the rheological experiment. However, when the most concentrated slurry ($C_{vf} = 0.292$) acted as the interstitial fluid, it was difficult to saturate sand particles with the slurry, thus C_{vc} was decreased to 0.474 in this case. Moreover, flow resistance of sand particles in air and in water were also measured for comparison, which were listed as sample 1 and sample 2 in Table 1.

2.2.2. Experimental setup and procedure

The vane geometry of the Physica MCR301 rheometer was used for rheological tests. It consists of a four-bladed vane and a profiled measuring cup (Fig. 3). Length of the vane is 16 mm. Radius of the vane is 11.01 mm. Radius of the cup is 21 mm.

The experiment included the following steps: (1) make the slurry and mix it thoroughly by hand; (2) put a measured amount of sand and slurry into the cup, then stir the mixture; (3) lower the vane to the measuring position where the vane is just immersed in the mixture; (4) keep the mixture undisturbed for 2 min to release the stress induced in step (3); (5) keep the vane rotating at a constant rate, and record the torque acting on the vane with an sampling frequency of 1–50 Hz until the torque remains stable; (6) lift the vane and mix the sample, then repeat steps (3)–(5) at another rotational rate. A circulating water bath was used to maintain the sample temperature at 20 ± 1 °C. Two rotational velocities, 0.05 rpm and 50 rpm, were examined to represent quasi-static state and high shear state, respectively. These tests were repeated once. Furthermore, more rotational speeds, spanning 0.05 rpm to 100 rpm, were investigated for sample 1, sample 7 and the slurry in sample 7 to study the influence of slurry on flow resistance at different shear rates.

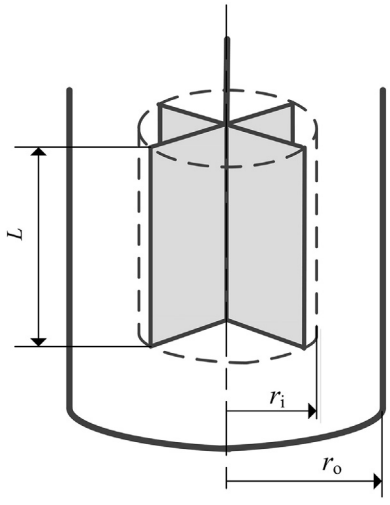

Fig. 3. Sketch map of the vane geometry.

Table 2
Natural angle of repose of gravels in different media in degree.

		In air		In water		In mud slurry	
Test number	Test method	Average	Standard deviation	Average	Standard deviation	Average	Standard deviation
1	Thread	41.95	1.77	42.15	1.53	42.66	2.77
	Triangle	40.33	0.56	43.08	2.28		
2	Thread	40.47	1.08	41.28	2.78		
	Triangle	41.46	0.61	43.09	1.27		

3. Experimental results and discussions

3.1. The natural angle of repose

Table 2 lists the experimental results on the natural angle of repose of gravels. Angles obtained with the thread method are equivalent to that acquired with the triangle method. The difference is within 2°, indicating the availability of the thread method. The angle of repose in mud slurry is slightly greater than that in air and in water. Taking the measurement error into consideration, these angles could be regarded as equivalent, which means the mud slurry generates little influence on the natural angle of repose of gravels.

3.2. Rheological tests

3.2.1. The torque-time response

3.2.1.1. $n = 0.05$ rpm. In the quasi-static case, the torque T acting on the vane varies with time t in three patterns. For samples 1–3, T decreases in the initial 3–5 min and then remains stabilized, as shown in Fig. 4. For samples 4–5, T decreases to a minimum at the first stage, and then it rises to a stable zone. The stable value is about 7%–13% higher than the minimum. For samples 6–8, T climbs up to a peak value in the first 1–2 min, then it decreases to a valley value and increases again to a stable region, as illustrated in Fig. 5. The stable value is at least 90% in excess of the valley value.

To analyze the data, the dimensionless number N defined by Ancey [18] to represent the relative importance of buoyant weight to yield

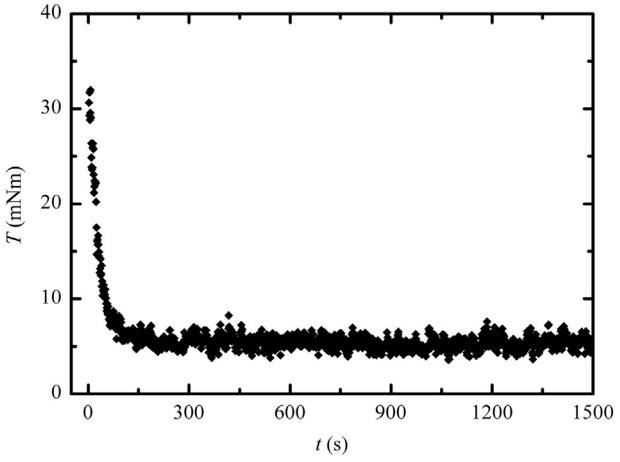

Fig. 4. Variation of torque T with time t for sample 1 at the rotational rate of 0.05 rpm.

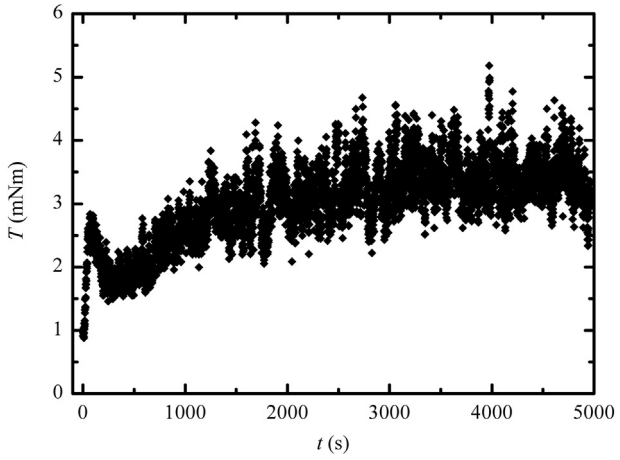

Fig. 5. Variation of torque T with time t for sample 7 at the rotational rate of 0.05 rpm.

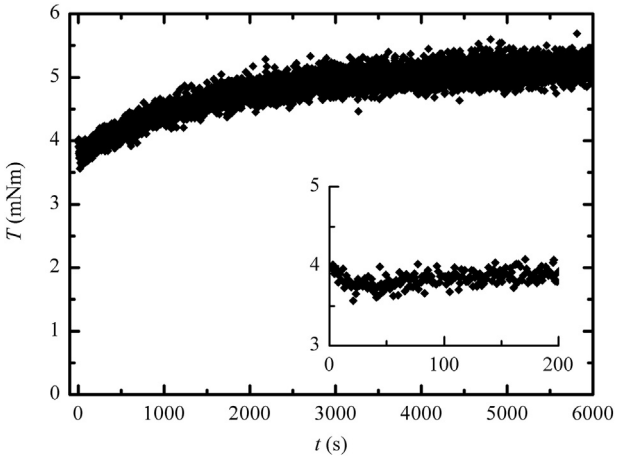

Fig. 6. Variation of torque T with time t for sample 1 at the rotational rate of 50 rpm.

strength was used as follows:

$$N = \frac{2C_{vc}\left(\rho_p - \rho_f\right)gR}{3\tau_{yf}} \quad (1)$$

where ρ_p is particle density, ρ_f is bulk density of the slurry, g is gravitational acceleration, R is particle radius, and τ_{yf} is yield strength of the slurry. Ancey [18] gives the following findings: when $N \gg 1$, the bulk behavior of the mixture is frictional at low shear rates and viscous at high shear rates; when $N \to 1$, the bulk behavior is time-dependent with viscoplastic properties in the short period and frictional properties in the long period; when $N < 1$, the mixture exhibits viscoplastic behaviors.

The value of N is computed for each sample with Eq. (1) and is listed in Table 1. For samples 2–5, $N \gg 1$, the yield strength is small and coarse particles settle quickly in the fluid, thus interparticle friction plays a dominant role in the quasi-static state just as the situation in the dry system (sample 1). After the sample is set in motion, the initial particle network is destroyed. It requires some time for particles in the shear zone to rearrange. Therefore, the torque drops in the first few minutes. The modest increase in torque during the later period for samples 4–5 is probably induced by partial settling of the fine particles in the slurry. For samples 6–7, $N \to 1$, the settling velocity of sand particles is quite small due to the relative high yield strength of the slurry. In the short term, coarse particles are suspended in the slurry, and the bulk behavior is viscoplastic. In this case, the torque initially increases with increasing shear strain and then decreases to a minimum after yielding, forming a peak in the torque profile in Fig. 5. This feature exhibited by some viscoplastic materials can be employed to determine the corresponding yield stress [22]. In the long term, with the settling of sand particles, excess pore fluid pressure gradually dissipates and thus the frictional force increases, generating the rise stage in the torque profile in Fig. 5. For sample 8, $N \ll 1$, the cohesive force of the slurry is large enough to keep coarse particles suspended and the mixture is expected to exhibit viscoplastic properties with the torque decreasing to a stable value after yielding. In fact, the torque exerted by sample 8 on the vane varies with time in the same pattern as that exerted by samples 6–7 in our experiment although it requires more time to reach the stable zone. This can be explained by the phenomenon that a thin layer of water formed during the test time, suggesting that the sample experienced structural settling and the excess pore fluid pressure had dissipated. Therefore, the frictional force also dominates in sample 8 at the end of the test.

3.2.1.2. $n = 50$ rpm. At the high shear state, the torque acting on the vane evolves with time in two patterns. For samples 1–6, T descends in the first 20 s, and then slowly ascends to a stabilized stage, as shown in Fig. 6. The time required to reach the stable area is 80–90 min for samples 1–4 and 30–40 min for samples 5–6. For samples 7–8, T only experiences a descending stage and then remains stable, as illustrated in Fig. 7. The decreasing stage lasts for 5–10 min for sample 7 and 60–70 min for sample 8.

The initial decrease in torque is attributed to the same reason as that in the quasi-static case, i.e., destruction of the particle network. Due to the increase in shear rate, this process is much shorter. The rising stage in Fig. 6 may result from particle migration. We found that particles in the center of the cup were coarser than other particles at the end of the test for samples 1–2, while it was difficult to check this phenomenon for the other samples due to the turbidity. In addition, we detected that the mixture was more concentrated at the bottom of the cup at the end of the test for all samples. However, further research is needed to investigate how particle migration affects the flow resistance. For samples 7–8, which exhibit viscoplastic behaviors at high rotational velocities, the rising stage in torque is absent although the mixture in the lower part of the cup was also found more concentrated when the test was finished. It indicates that particle migration produces different impacts on the flow resistance of viscoplastic mixtures and frictional mixtures.

3.2.2. Effects of the slurry on the flow resistance at $n = 0.05$ rpm and $n = 50$ rpm

For each sample, both the stable torque T_{sta} and the minimum torque T_{min} are computed in the case of $n = 0.05$ rpm and $n = 50$ rpm, respectively. T_{sta} is defined as the average of torques in the stable region of the $T \sim t$ plot. If T experiences a valley region in the $T \sim t$ plot, T_{min} is defined as the minimum average of torques sampled in 1 min. If T starts with a

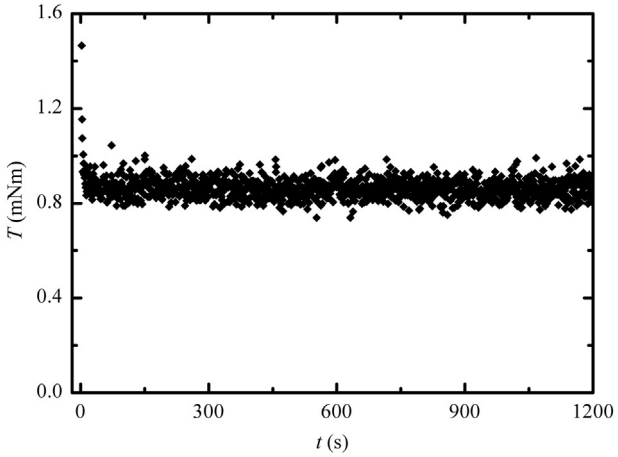

Fig. 7. Variation of torque T with time t for sample 7 at the rotational rate of 50 rpm.

decreasing period and then remains stable, T_{min} is equal to T_{sta}. Repeated tests suggest that the repeatability in T_{min} and T_{sta} is <20%, and in most cases it is <10%.

Mean values of the corresponding statistics in the two tests are used to compare flow resistance of each sample. The results are shown in Fig. 8. For all samples, flow resistance at $n = 50$ rpm is lower than that at $n = 0.05$ rpm. This may derive from two factors. One is destruction of the particle network is more thorough at the high rotational speed. The other is excess pore fluid press is higher at the high shear state. When $N = 0.05$ rpm, T_{min} generally decreases with the increase in slurry density and exhibits three grades. T_{min} for sample 1 is the highest with a value of 6.01 mNm. Values of T_{min} for samples 2–5 are medium and range from 3 mNm to 4 mNm, which corresponds with the role of interstitial fluids in decreasing the effective normal stress and thus reducing the frictional force. Values of T_{min} for samples 6–8 are low, varying between 1 mNm and 2 mNm. It indicates that when the viscoplastic force plays a dominant role the flow resistance can be further reduced. In terms of the stable torque, the difference is small. Values of T_{sta} range from 3 mNm to 4 mNm for all samples except sample 1. It shows that the slurry concentration does not have significant influence on the flow resistance after the excess pore fluid pressure has dissipated. When $n = 50$ rpm, T_{min} diminishes with the rise in slurry concentration as that in the case of $N = 0.05$ rpm. However, it does not exhibit the characteristic of falling into several grades.

When the bulk behavior of the mixture is frictional, the flow resistance is proportional to the effective normal stress. In this case, the torque acting on the vane, consisting of the torque acting on the wall of the imaginary cylinder and the torque acting on the lower end of the cylinder [23], can be expressed as:

$$T = \mu\pi r_i^2 L^2 g C_{vc}\left(\rho_p - \rho_f\right)\left(k + \frac{2r_i}{3L}\right) \tag{2}$$

in which μ and k are the internal friction coefficient and the lateral pressure coefficient of sand particles, respectively, r_i is radius of the vane, and L is length of the vane. Then we can define the dimensionless torque T' as:

$$T' = \frac{T}{\pi r_i^2 L^2 g C_{vc}\left(\rho_p - \rho_f\right)} = \mu\left(k + \frac{2r_i}{3L}\right). \tag{3}$$

In the present study, it is reasonable to suppose that k remains constant from one test to another, especially for the tests with the same rotational velocity, in which case the samples have undergone similar deformation processes. As a consequence, in Eq. (3) T' is proportional to μ, and the variation of T' with slurry concentration can be employed to reflect the influence of the slurry concentration on μ.

The corresponding dimensionless torques, T'_{min} and T'_{sta}, are computed with the first part of Eq. (3) respectively and illustrated in Fig. 9. When $n = 0.05$ rpm, samples 6–8 exhibit viscoplastic behaviors in the short term, and their T'_{min} values are far less than the dry system, only 46%–67% compared with that of sample 1. As to samples 2–5, they have similar T'_{min} values with sample 1. In the long term, the bulk behavior of samples 6–8 is frictional, and values of T'_{sta} are remarkably higher than T'_{min}. In this case, T'_{sta} value of sample 6 is close to sample 1, while sample 7 and sample 8 have T'_{sta} values 30% greater than sample 1. Rheological tests using the vane tool on the mud slurries with $C_{vf} = 0.243$ and $C_{vf} = 0.292$ show that the torques are always below 0.1 mNm in the case of $n = 0.05$ rpm, which means that the torque contributed by the slurry itself accounts for <4% in the total stable torque for samples 7–8 at the low rotational velocity. The fact that samples 7–8 have higher T'_{sta} values than the other samples is probably caused by the increase in the total solid concentration C_{vt} (Table 1), which can enhance the compactness of the solid particles and thus increase the internal friction coefficient. The phenomenon that T'_{sta} values of samples 1–6 are close to each other reveals that the mud slurry has no evident effects upon the frictional coefficient of silica sands. This agrees with the experimental results on the angle of repose. When $n = 50$ rpm, the dimensionless torque values of samples 2–4 are slightly lower than the dry system, with the difference within 15%. By contrast, the corresponding values of samples 5–8 are much less than sample 1, with the difference beyond 30%. It indicates that even if the cohesive strength of the slurry is insufficient to maintain the silica sand suspended, the settling of sands is dampened to some extent at the high shear rate, and the excess pore fluid pressure is partially preserved. The higher the cohesive strength of the slurry, the higher the excess pore fluid pressure is, thereby generating a more significant effect in reducing flow resistance.

3.2.3. Effects of the slurry on flow resistance at different rotational velocities

Rheological tests were performed on sample 7 to detect the torque-time response at 11 different rotational velocities ranging between 0.05 rpm and 100 rpm. Results show that when $n \le 22$ rpm the torque experiences a similar process to that detected at $n = 0.05$ rpm (Fig. 5), and the time required to reach the stable stage decreases with increasing rotational speed, with 50 min at $n = 0.05$ rpm and 6 min at $n = 22$ rpm. When $n > 22$ rpm, the torque evolves similarly to the case at $n = 50$ rpm (Fig. 7). Both T_{min} and T_{sta} are plotted versus the rotational velocity in Fig. 10. T_{min} decreases with the increase in rotational velocity at low velocities ($n \le 0.5$ rpm) and increases at high velocities, while T_{sta} decreases monotonously with increasing rotational speed.

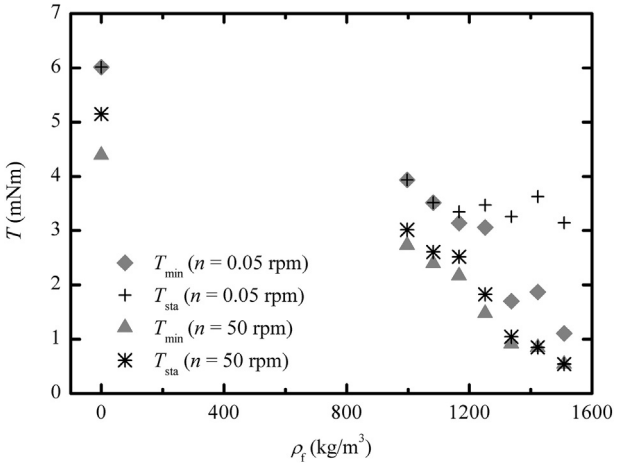

Fig. 8. The minimum torque T_{min} and stable torque T_{sta} as functions of the slurry density ρ_f.

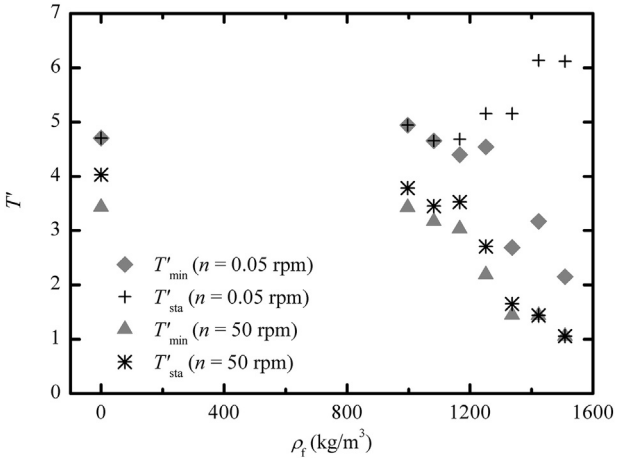

Fig. 9. The dimensionless minimum torque T'_{min} and stable torque T'_{sta} as functions of the slurry density ρ_f.

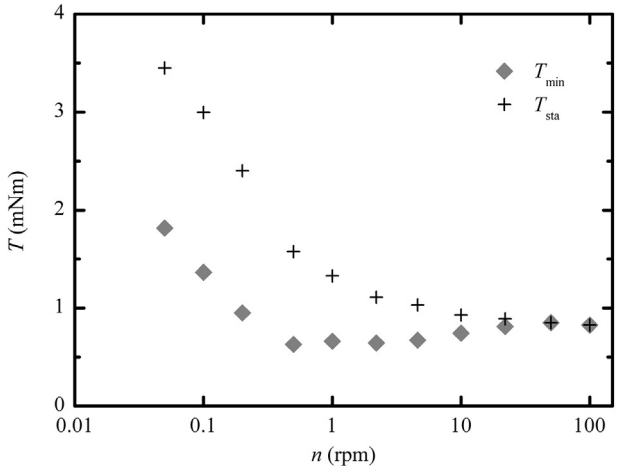

Fig. 10. The minimum torque T_{min} and stable torque T_{sta} as functions of rotational rate n for sample 7.

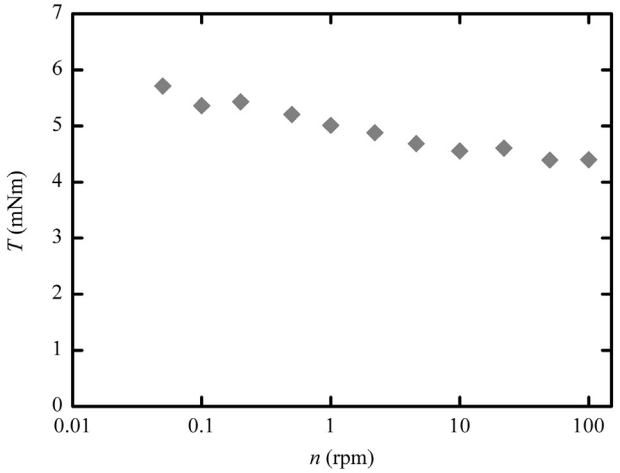

Fig. 12. The minimum torque T as a function of rotational rate n for sample 1.

T_{min} represents the bulk behavior of the mixture in the short term, which generally approximates that of the interstitial fluid [18]. Rheological tests on the corresponding slurry demonstrate that the stable torque increases monotonously with increasing rotational speed, as shown in Fig. 11. At low shear rates, the structural strength of the slurry-sand mixture dominates in flow resistance in the short term. The structure is destroyed more thoroughly with the increase in shear rate. At high shear rates, viscous force plays an increasingly important role, which increases with shear rate. This can explain the inconsistence in bulk behaviors of the mixture and the slurry.

T_{sta} represents the bulk behavior of the mixture in the long term, which is expected to be frictional at low shear rates and viscous at high shear rates [18]. Fig. 10 illustrates that T_{sta} equals to T_{min} at $n =$ 50 rpm and $n = 100$ rpm, indicating that the viscous force dominates in these two cases. Rheological tests on the dry system show that when $n \le 1$ rpm the torque profile is similar to that obtained at $n =$ 0.05 rpm (Fig. 4) while it is similar to that obtained at $n = 50$ rpm (Fig. 6) when $n > 1$ rpm. The torque has not reached the stable stage during the test time at some rotational velocities. Therefore, only T_{min} is plotted versus rotational rate in Fig. 12, suggesting that T_{min} decreases with increasing rotational rate. Experimental results on the rheological behavior of dry particles in the present research are different from some findings in the literature [24–25], which indicate that shear stress is independent of shear rate at low shear rates while it increases with shear rate at high shear rates. The inconsistence most likely results from the particle migration observed in our experiment and needs further study. For sample 7, the variation of T_{sta} with rotational rate exhibits the same trend as that illustrated in Fig. 12, whereas T_{sta} decreases more sharply. For example, T_{sta} at $n = 10$ rpm is 27% of the value at $n = 0.05$ rpm for sample 7, while the corresponding proportion is 80% for sample 1. It reveals that the increase in shear rate tends to reduce the settling of sand particles and maintain the excess pore fluid pressure, thus decreasing the frictional force significantly. When $n =$ 50 rpm, all of the excess pore fluid pressure can be maintained and the sand-slurry mixture behaves as a viscoplastic fluid.

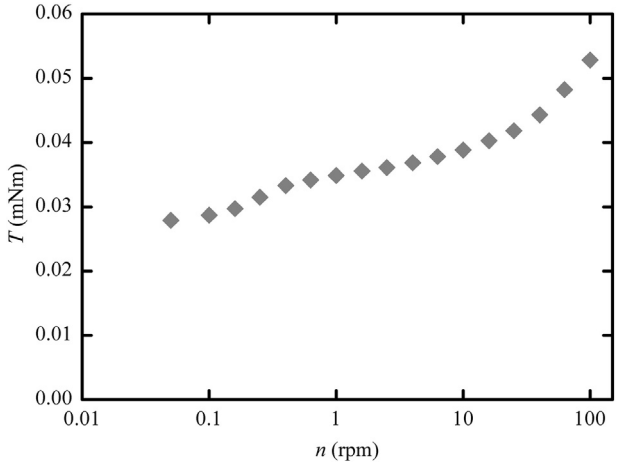

Fig. 11. The stable torque T as a function of rotational rate n for the mud slurry with $C_{vf} =$ 0.243.

3.3. Discussions

Making laboratory tests simulate real debris flow conditions is not easy. This is mainly because solid particles in debris flow are poorly sorted and cover a wide size range varying from clay minerals to boulders. It is difficult to satisfy both geometric similarity and dynamic similarity in small-scale experiments [26]. In our rheological experiment, the coarse particles are relatively homogeneous in size, and the total solid concentration changes between 0.506 and 0.627. In contrast, the bulk density of high-density, high-viscosity debris flow pulses is generally >2100 kg/m^3 [27], which is equivalent to the solid volume concentration of ~0.67. Consequently, it is most likely that excess pore fluid pressure is more difficult to dissipate in real debris flows for the smaller porosity. Moreover, the vane utilized in the test is 16 mm in length, while the depth of real debris flows is usually measured in meters. Hence, the normal stress in the test is much smaller than the natural case. However, we analyzed the experimental results with the dimensionless number T', thus their availability is not limited to the experimental scale.

For the limitation of the experimental instrument, excess pore fluid pressure was not directly measured in this study. We deduced the existence of excess pore fluid pressure from the detected torque-time response and the formation of a thin layer of water at the surface of the sample during test. Nonetheless, the significance of excess pore fluid pressure in debris flows have been demonstrated in both field and laboratory work [13–14,28]. Large-scale flume experiments have been conducted by Iverson et al. [14] to investigate flow mobility of two sediment mixtures: sand-gravel mixture and sand-gravel-mud mixture. They suggest that debris flows simulated with the sand-gravel-mud mixture have higher mobility by maintaining high pore pressures in flow bodies. Another example to demonstrate the important role of mud in enhancing flow mobility can be found by analyzing field measurement data. Data collected from 5 debris flow gullies in China show that surge velocity increases with increasing clay content in the sediment [29].

4. Conclusions

In this research the influence of mud slurry on the flow resistance of cohesionless particles was studied by means of rheological tests and experiments on the angle of repose. Measurements suggest that the slurry has no obvious effects upon the internal friction angle of coarse particles. However, it can reduce the flow resistance via two mechanisms. On the one hand, the slurry has higher bulk density than water, thus the buoyant weight of the particle is decreased. On the other hand, existence of the slurry tends to maintain the excess pore fluid pressure and make the particles partially or completely liquefied. It becomes difficult for excess pore fluid pressure to dissipate when yield strength of the slurry is high or the shear rate is high, thus the flow resistance can be decreased significantly. Once the particles are fully liquefied, the whole mixture behaves as a viscoplastic fluid.

Conclusions from this research are mainly qualitative. To apply them in the dynamic simulation of debris flow, quantitative study should be conducted to examine how cohesive strength of the slurry and shear rate influence the dissipation of excess pore fluid pressure in the future.

Acknowledgements

This work was financially supported by the National Natural Science Foundation of China (grant no. 41201011), the Key Research Program of the Chinese Academy of Sciences (CAS) (grant No. KZZD-EW-05-01), and the Youth Talent Team Program of Institute of Mountain Hazards and Environment, CAS (grant no. SDSQB-2013-01). The authors are grateful to the reviewers for providing constructive comments.

References

[1] M. Preisig, T. Zimmermann, Two-phase free-surface fluid dynamics on moving domains, J. Comput. Phys. 229 (2010) 2740–2758.
[2] X. Fei, G. Xiong, Energy dissipation and calculation of resistance and velocity of debris flow, Int. J. Sediment Res. 12 (1997) 65–73.
[3] E.B. Pitman, L. Le, A two-fluid model for avalanche and debris flows, Phil. Trans. R. Soc. A 363 (2005) 1573–1601.
[4] R.M. Iverson, D.L. George, A depth-averaged debris-flow model that includes the effects of evolving dilatancy. I. Physical basis, Proc. R. Soc. A 470 (2014) http://dx.doi.org/10.1098/rspa.2013.0819.
[5] T. Takahashi, Debris Flow: Mechanics, Prediction and Countermeasures, Taylor and Francis, Leiden, 2007 1–102.
[6] P. Coussot, D. Laigle, M. Arattano, A. Deganutti, L. Marchi, Direct determination of rheological characteristics of debris flow, J. Hydraul. Eng. 124 (1998) 865–868.
[7] P. Coussot, J.-M. Piau, On the behavior of fine mud suspensions, Rheol. Acta 33 (1994) 175–184.
[8] R. Sosio, G.B. Crosta, Rheology of concentrated granular suspensions and possible implications for debris flow modeling, Water Resour. Res. 45 (2009), W03412.
[9] G. MiDi, On dense granular flows, Eur. Phys. J. E 14 (2004) 341–365.
[10] Y. Forterre, O. Pouliquen, Flows of dense granular media, Annu. Rev. Fluid Mech. 40 (2008) 1–24.
[11] J.M.N.T. Gray, C. Ancey, Multi-component particle-size segregation in shallow granular avalanches, J. Fluid Mech. 678 (2011) 535–588.
[12] B.P. Kokelaar, R.L. Graham, J.M.N.T. Gray, J.W. Vallance, Fine-grained linings of leveed channels facilitate runout of granular flows, Earth Planet. Sci. Lett. 385 (2014) 172–180.
[13] T. Ilstad, J.G. Marr, A. Elverhøi, C.B. Harbitz, Laboratory studies of subaqueous debris flows by measurements of pore-fluid pressure and total stress, Mar. Geol. 213 (2004) 403–414.
[14] R.M. Iverson, M. Logan, R.G. LaHusen, M. Berti, The perfect debris flow? Aggregated results from 28 large-scale experiments, J. Geophys. Res. 115 (2010), F03005.
[15] N. Jain, J.M. Ottino, R.M. Lueptow, Effect of interstitial fluid on a granular flowing layer, J. Fluid Mech. 508 (2004) 23–44.
[16] H.T. Chou, S.H. Chou, S.S. Hsiau, The effects of particle density and interstitial fluid viscosity on the dynamic properties of granular slurries in a rotating drum, Powder Technol. 252 (2014) 42–50.
[17] F. Boyer, É. Guazzelli, O. Pouliquen, Unifying suspension and granular rheology, Phys. Rev. Lett. 107 (2011) 188301.
[18] C. Ancey, Role of lubricated contacts in concentrated polydisperse suspensions, J. Rheol. 45 (2001) 1421–1439.
[19] K. Hutter, T. Koch, Motion of a granular avalanche in an exponentially curved chute: experiments and theoretical predictions, Philos. Trans. R. Soc. Lond. Ser. A 334 (1991) 93–138.
[20] S. Zhang, A comprehensive approach to the observation and prevention of debris flows in China, Nat. Hazards 7 (1993) 1–23.
[21] H. Yang, F. Wei, K. Hu, G. Zhou, J. Lyu, Comparison of rheometric devices for measuring the rheological parameters of debris flow slurry, J. Mt. Sci. 12 (2015) 1125–1134.
[22] F. Mahaut, X. Chateau, P. Coussot, G. Ovarlez, Yield stress and elastic modulus of suspensions of noncolloidal particles in yield stress fluids, J. Rheol. 52 (2008) 287–313.
[23] H.A. Barnes, Q.D. Nguyen, Rotating vane rheometry - a review, J. Non-Newtonian Fluid Mech. 98 (2001) 1–14.
[24] R.C. Daniel, A.P. Poloski, A.E. Sáez, Vane rheology of cohesionless glass beads, Powder Technol. 181 (2008) 237–248.
[25] P. Mort, J.N. Michaels, R.P. Behringer, C.S. Campbell, L. Kondic, M.K. Langroudi, M. Shattuck, J. Tang, G.I. Tardos, C. Wassgren, Dense granular flow-a collaborative study, Powder Technol. 284 (2015) 571–584.
[26] R.M. Iverson, The physics of debris flows, Rev. Geophys. 35 (1997) 245–296.
[27] T.R.H. Davies, Large debris flows: a macro-viscous phenomenon, Acta Mech. 63 (1986) 161–178.
[28] S.W. McCoy, J.W. Kean, J.A. Coe, D.M. Staley, T.A. Wasklewicz, G.E. Tucker, Evolution of a natural debris flow: in situ measurements of flow dynamics, video imagery, and terrestrial laser scanning, Geology 38 (2010) 735–738.
[29] H. Yang, F. Wei, K. Hu, Mean velocity estimation of viscous debris flows, J. Earth Sci. 25 (2014) 771–778.

Hongjuan Yang is an associate professor in Institute of Mountain Hazards and Environment, Chinese Academy of Sciences. She received her Ph.D. in Hydraulic Engineering from Tsinghua University in 2009. Her research is focused on rheology of granular suspensions and debris flow dynamics.

Fangqiang Wei is a professor in Institute of Mountain Hazards and Environment, Chinese Academy of Sciences. He received his Ph.D. in geotechnical engineering from Southwest Jiaotong University in 2002. His research is focused on forecasting of mountain hazards and technology for disaster mitigation.

Kaiheng Hu is a professor in Institute of Mountain Hazards and Environment, Chinese Academy of Sciences. He received his Ph.D. in fluid mechanics from Peking University in 2006. His research interests include theory and technology for debris flow mitigation, and numerical simulation of debris flow.

Juan Lyu is a senior engineer in Institute of Mountain Hazards and Environment, Chinese Academy of Sciences. Her attention has been focused on the monitoring, simulation, and rheology of debris flow for more than 20 years.